SUPPORTING INFORMATION

Highly selective and sensitive fluorogenic detection of GSH using mesoporous silica nanoparticles capped with disulfide-containing oligo(ethylene glycol) chains

Sameh El Sayed, Cristina Giménez, Ramón Martínez-Máñez, Félix Sancenón and Maurizio Licchelli

Reagents:

The chemicals tetraethylorthosilicate (TEOS), n-cetyltrimethylammonium bromide (CTABr), sodium hydroxide (NaOH), Safranine O, (3-mercaptopropyl) trimethoxysilane, 2,2'-dipyridyl disulfide, *O*-(2-Mercaptoethyl)-*O*'-methyl-hexa(ethylene glycol), GSH and selected amino acids (Cys, Hcy, Ala, Arg, Asn, Asp, Glu, Gln, Gly, His, Thr, Trp, Tyr and Val) were provided by Sigma-Aldrich. Human serum from male AB plasma, USA origin were provided by Sigma-Aldrich. Analytical-grade solvents were from Scharlab (Barcelona, Spain). All reagents were used as received.

Methods:

X-ray measurements were performed on a Brücher AXS D8 Advance diffractometer using Cu-Kα radiation. Thermo gravimetric analysis were carried out on a TGA/SDTA 851e Mettler Toledo equipment, using an oxidant atmosphere (Air, 80 mL/min) with a heating program consisting on a heating ramp of 10 °C per minute from 393 K to 1273 K and an isothermal heating step at this temperature for 30 minutes. TEM images were taken with a JEOL TEM-1010 Electron microscope working at 100 kV. N_2 adsorption-desorption isotherms were recorded on a Micromeritics ASAP2010 automated sorption analyser. The samples were degassed at 120ºC in vacuum overnight. The specific surfaces areas were calculated from the adsorption data in the low pressures range using the BET model. Pore size was determined following the BJH method. Fluorescence spectroscopy was carried out on a Jasco FP-8300 Spectrometer and UV-visible spectroscopy was carried out with a Jasco V-630 Spectrometer.

Synthesis of the silica mesoporous nanoparticles support (SMPS)

n-cetyltrimethylammoniumbromide (CTABr, 1.00 g, 2.74 mmol) was first dissolved in 480 mL of distilled water. Then a 3.5 mL of NaOH 2.00 M in distilled water was added to the CTABr solution, followed by adjusting the solution temperature to 80ºC. TEOS (5 mL, 2.57×10^{-2} mol) was then added drop wise to the surfactant solution. The mixture was stirred for 2 h and white precipitate was obtained. Finally the precipitate was centrifuged, washed with distilled water and dried at 60ºC (MCM-41 as-synthesized). To prepare the final porous material (MCM-41), the as-synthesized solid was calcined at 550 ºC using oxidant atmosphere for 5 h in order to remove the template phase.

Synthesis of S1

500 mg of calcined MCM-41 and safranin O dye (140.34 mg, 0.40 mmol) were suspended in acetonitrile (17 mL) in a round-bottomed flask. The mixture was stirred for 24 h at room temperature, filtered off and dried under vacuum. Afterward, this loaded solid (250 mg) was re-suspended in acetonitrile (8.5 mL) in the presence of an excess of safranin O and (3-mercaptopropyl) trimethoxysilane (464.38 µL, 2.5 mmol) was added. The suspension was stirred for 5.5 h at room temperature and then, 2,2'-dipyridyl disulfide (550.77 mg, 2.5 mmol) was added to the reaction mixture. After stirring for 12 h at room temperature, the resulting solid was filtered off and dried under vacuum. Finally, a mixture of this prepared solid (50 mg) and *O*-(2-Mercaptoethyl)-*O*'-methyl-hexa(ethylene glycol) (0.14 mmol) were suspended in acetonitrile (3.33 mL) in the presence of an excess of safranin O. The mixture was stirred for 12 h and the final support **S1** was isolated by centrifugation, washed with abundant water and dried at 40 ºC for 12 h.

Materials Characterization

MCM-41, calcined MCM-41, and **S1** were characterized through standard techniques. Figure S1 shows the X-ray diffraction (XRD) patterns of the as-synthesized MCM-41 matrix, the calcined MCM-41, and the final **S1** solid. Plain MCM-41 (curve a) displayed the four typical low-angle reflections of a hexagonal-ordered matrix indexed at (100), (110), (200) and (210) Bragg peaks. In curve b, calcined MCM-41 shows a significant shift of the (100) peak in the PXRD and a broadening of the (100) and (200) peaks. These changes are due to the condensation of silanols in the calcination step, which caused an approximate cell contraction of 4 Å. Finally, curve c) shows the PXRD pattern of **S1** solid. For this material, reflections (110) and (2 00) were mostly lost due to a reduction in contrast related to the functionalization process and to the filling of mesopores with safranin O. Even so, the intensity of the (100) peak in this pattern strongly indicates that the loading process with the dye and the additional functionalization with the oligo(ethylene glycol) chains did not modify the mesoporous MCM -41 scaffold.

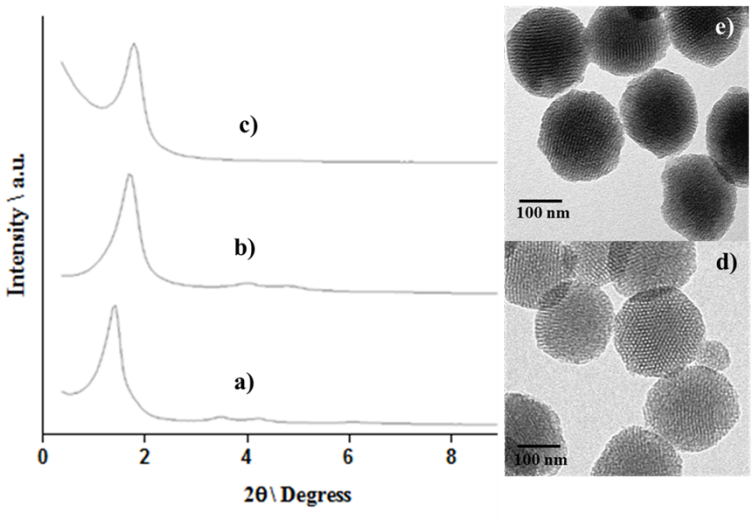

Fig. S1. X-ray patterns of (a) MCM-41, (b) calcined MCM-41 and (c) **S1**. TEM images of (d) calcined MCM-41 and (e) **S1**.

Moreover, TEM images of the investigated solid materials show the typical channels of the MCM-41 matrix as alternate black and white stripes. The typical hexagonal porosity of the calcined MCM-41 material can also be observed (Figure S1-d). TEM images also show that calcined MCM-41 was obtained as spherical nanoparticles with diameters between 80 and 100 nm. Shape and dimension of nanoparticles were preserved even after loading and functionalization processes (Figure S1-d-e).

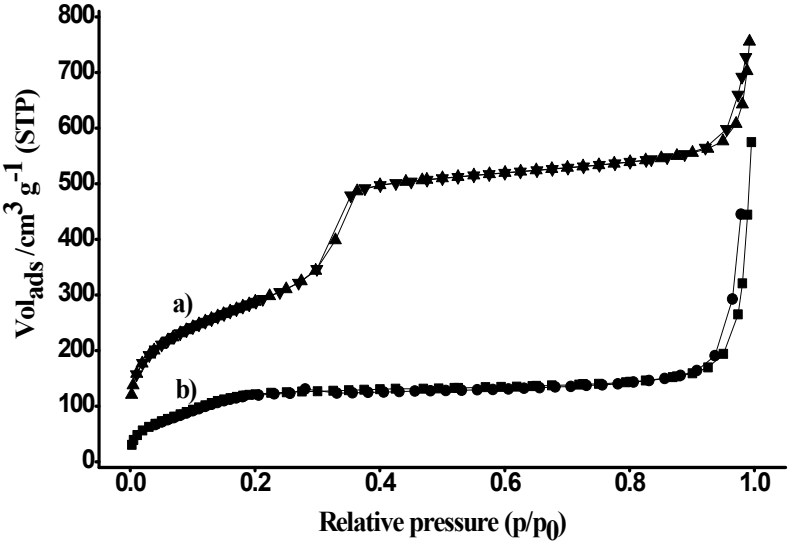

Fig. S2. Nitrogen adsorption-desorption isotherms for (a) MCM-41 mesoporous material and (b) **S1** material.

Figure S2 (curve a) shows the N_2 adsorption-desorption isotherms of the calcined MCM-41 nanoparticles. This curve displays an adsorption step with a P/P0 value between 0.2 and 0.35, corresponding to a type IV isotherm, which is typical of mesoporous materials. This first step is due to nitrogen condensation in the mesopore inlets. With the BJH model on the adsorption curve of the isotherm, the pore diameter and pore volume were calculated to be 2.76 nm and 0.9 $cm^3\ g^{-1}$, respectively. The absence of a hysteresis loop in this pressure range and the low BJH pore distribution is due to the cylindrical uniformity of mesopores. The total specific area was 1045.70 $m^2\ g^{-1}$, calculated with the BET model. The a_0 cell parameter (44.58 nm) and the wall thickness (16.98 Å) were calculated from the PXRD, porosimetry and TEM measurements. Other important feature of the curve is the characteristic H1 hysteresis loop that appears in the isotherm at a high relative pressure (P/P 0> 0.8), which can be closely associated with a wide pore size distribution. This corresponds to the filling of the large pores among the nanoparticles (0.75 $cm^3\ g^{-1}$ calculated by the BJH model) due to textural porosity. On the other hand, for the **S1** material, the N_2 adsorption-desorption isotherm is typical of mesoporous systems with partially filled pores (see Figure S2,

curve b). In this way, and as it can be expected, a lower N_2 adsorbed volume (BJH mesopore volume = 0.28 $cm^3 g^{-1}$) and surface area (491.1 $m^2 g^{-1}$) were found, when compared with the initial MCM-41 material. As observed, this solid presents a curve with no gaps at low relative pressure values if compared to the mother MCM-41 matrix (curve a). Another important feature of **S1** is that no maximum was observed in the pore size distribution curve, which can be explained by the presence of closed pores (see Figure S3 for pore size distributions).

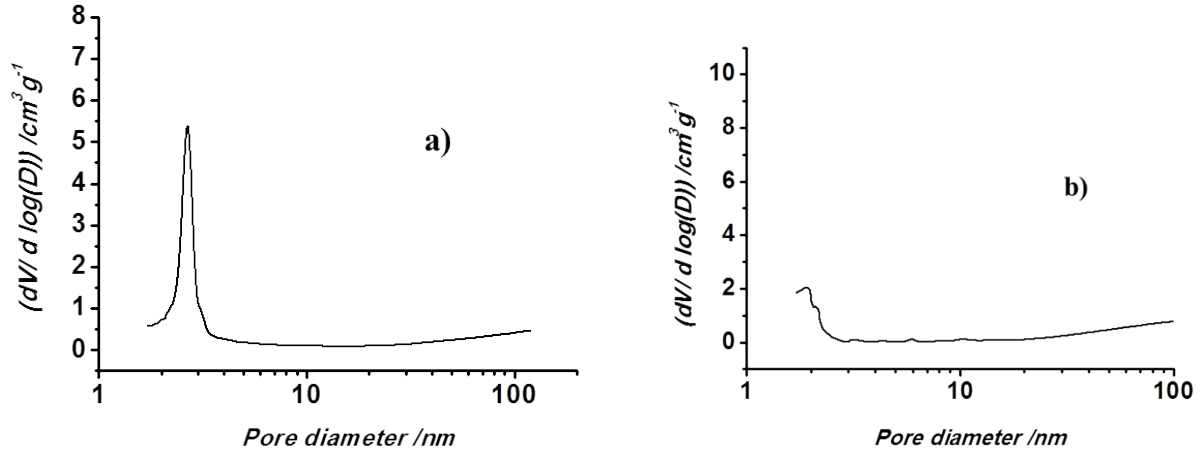

Fig. S3. Pore size distributions for (a) Calcined MCM-41mesoporous material (b) **S1**.

Thermogravimetric studies of **S1** showed the existence of three weights loss steps (see Figure S4); i.e. weight losses of 6.74 % ($T < 150\ ^0C$, corresponding to solvent elimination), 28.10 % ($300 < T < 550\ ^0C$) due to combustion of organics) and 2.09 % ($T > 550\ ^0C$, attributed to condensation of silanols in the siliceous surface) were observed. Also dynamic light scattering studies with MCM-41 calcined and the final **S1** solid were carried out (see Figure S4). As seen in the figure MCM-41 calcined and **S1** presented mean diameters of ca. 85 and 150 nm respectively.

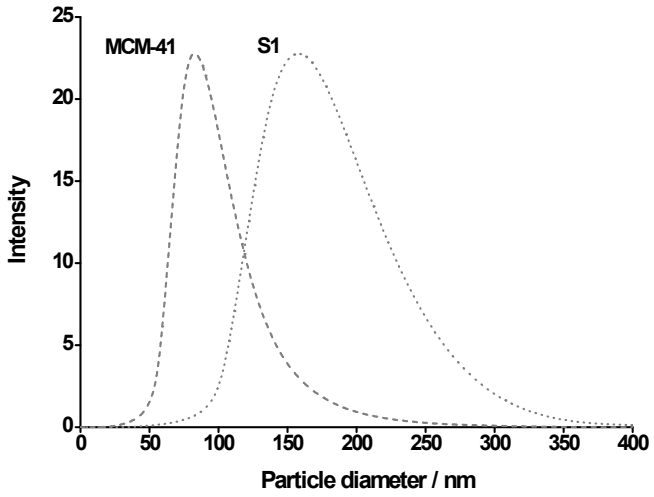

Fig. S4. Size distribution by number of particles obtained by DLS studies for calcined MCM-41 and **S1**solids.

Selectivity of the method, was studied via monitoring the response of **S1** in the presence of 10 mM of selected anions (HS^-, F^-, Br-, Cl^-, I^-, CN^-, OH^-, HPO_4^-, AcO^-, Citrate, N_3^-, NO_3^{-2}, SO_3^{-2}, SO_4^{-2} and $S_2O_4^{-2}$), oxidants (H_2O_2), amino acids (Hcy, Cys, Me-Cys, Ala, Arg, Asn, Asp, Glu, Gln, Gly, His, Thr, Trp, Tyr and Val), GSH, ME and DTT. Dye delivery from **S1** after 30 min upon guest addition is shown in Figure 3 in the main text. Moreover Figure S5 shows the response of **S1** to GSH in competitive experiments for mixtures of GSH (10 mM) alone and mixtures containing GSH (10 mM) and 10 mM of different anions, oxidants, amino acids and Me-Cys, Cys or Hcy.

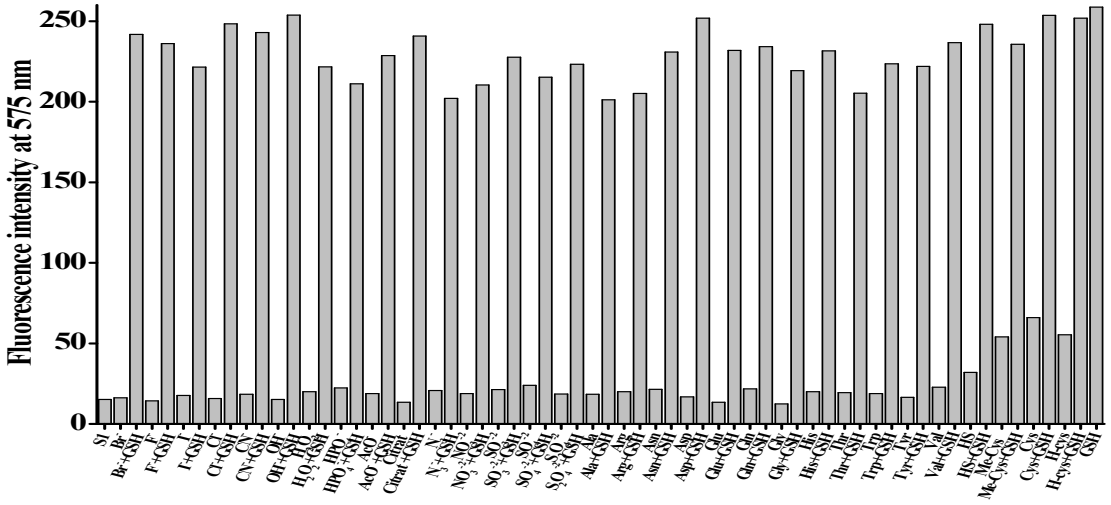

Fig. S5. Fluorescence intensity at 575 nm (λ_{ex} 520 nm) of safranin O dye released from **S1** in water pH 7.0 after 30 min upon addition of 10 mM of GSH alone and in the prescence of 10 mM of GSH + 10 mM of anions, cations oxidants, reducing agents, phosphates , amino acids, Me-Cys, Cys, Hcy and GSH.

Human serum GSH serve as an accurate indicator of GSH status in human subjects and play an important role in some diseases. Thus, the development of simple and accurate analytical method for the determination of GSH is of interest. We attempted to detect SGH using **S1** in more complex systems and selected human serum and artificial serum as more realistic environment. Results obtained using human serum are shown in Table 1 of the manuscript. Moreover here we describe the results obtained in artificial serum. Artificial serum was prepared according to a well-established protocol[1] and it was spiked with conventional quantities of biothiols (Cys: 178.4 μM; Hcy: 5.9 μM and GSH (2.5, 4, 6, 10 μM)). SGH content in the samples was determined using **S1** and following the method of standard addition. Results are shown in Table S1. As seen in the table, **S1** was satisfactorily applied to the detection of GSH with high recovery ratios ranging from 92 to 118 %.

Table S1. Determination of GSH in artificial serum.

Sample	GSH spiked (μM)	GSH measured (μM)	Recovery (%)
1	2.5	2.3±0.15	92
2	4.0	4.3±0.24	107
3	6.0	7.1±0.35	118
4	10.0	9.4±0.86	94

[ ] For serum preparation see: M. R. C. Marques, R. Loebenberg, M. Almukainzi, *Dissolution Technol*., 2011, **18**, 15.